AGU PUBLICATIONS

JGR

Journal of Geophysical Research: Space Physics

RESEARCH ARTICLE
10.1002/2015JA022056

Key Points:
- Beating of the lunar and solar semidiurnal tides leads to an equatorial vertical drift modulation
- The strong modulation is observable at Jicamarca during the 2013 SSW
- The lunar and solar semidiurnal tides have comparable amplitudes leading to strong drift modulation

Correspondence to:
A. Maute,
maute@ucar.edu

Citation:
Maute, A., B. G. Fejer, J. M. Forbes, X. Zhang, and V. Yudin (2016), Equatorial vertical drift modulation by the lunar and solar semidiurnal tides during the 2013 sudden stratospheric warming, *J. Geophys. Res. Space Physics*, *121*, 1658–1668, doi:10.1002/2015JA022056.

Received 19 OCT 2015
Accepted 26 JAN 2016
Accepted article online 29 JAN 2016
Published online 19 FEB 2016

Equatorial vertical drift modulation by the lunar and solar semidiurnal tides during the 2013 sudden stratospheric warming

A. Maute[1], B. G. Fejer[2], J. M. Forbes[3], X. Zhang[3], and V. Yudin[4,5]

[1]High Altitude Observatory, National Center for Atmospheric Research, Boulder, Colorado, USA, [2]Center for Atmospheric and Space Sciences, Utah State University, Logan, Utah, USA, [3]Department of Aerospace Engineering Sciences, University of Colorado Boulder, Boulder, Colorado, USA, [4]Cooperative Institute for Research in Environmental Sciences, University of Colorado Boulder, Boulder, Colorado, USA, [5]Atmospheric Chemistry Observations and Modeling, National Center for Atmospheric Research, Boulder, Colorado, USA

Abstract During the 2013 stratospheric sudden warming (SSW) period the Jicamarca Unattended Long-term Investigations of the Ionosphere and Atmosphere (JULIA) radar at Jicarmarca, Peru, observed low-latitude vertical drift modulation with lows of 0–12 m/s daytime maximum drifts between 6–13 and 22–25 January and enhanced drifts up to 43 m/s between 15 snd 19 January. The NCAR thermosphere-ionosphere-mesosphere-electrodynamics general circulation model reproduces the prevailing vertical drift feature and is used to examine possible causes. The simulations indicate that the modulation of the vertical drift is generated by the beating of the semidiurnal solar SW_2 and lunar M_2 tides. During the SSW period the beating is observable since the magnitudes of lunar and solar semidiurnal tidal amplitudes are comparable. The theoretical beating frequency between SW_2 and M_2 is 1/(15.13 day) which may be modified due to phase changes. This study highlights the importance of the lunar tide during SSW periods and indicates that the equatorial vertical drift modulation should be observable at other longitudes as well.

1. Introduction

Stratospheric sudden warmings (SSW) are caused by large changes in the lower atmosphere which effects may be observable in the thermosphere-ionosphere system [e.g., *Goncharenko and Zhang*, 2008; *Chau et al.*, 2009; *Vineeth et al.*, 2009; *Pedatella and Forbes*, 2010; *Lin et al.*, 2012; *Pancheva et al.*, 2012]. The ionospheric wind dynamo is one of the possible mechanisms of linking changes in the lower to the upper atmosphere. Daytime *E* region winds are very effective in generating electric fields which can modify the vertical drift and the distribution of *F* region plasma [e.g., *Chau et al.*, 2009; *England*, 2012].

During SSW periods large planetary wave activity is present in the winter polar stratosphere, which causes the eastward polar jet to weaken or even reverse direction. The deceleration in the polar wind leads to vertical wind divergence with adiabatic heating in the stratosphere due to downward winds and adiabatic cooling in the mesosphere due to upward winds [e.g., *Matsuno*, 1971]. The disturbed middle atmosphere alters the wave and tidal propagation [e.g., *Forbes et al.*, 2013; *Pedatella et al.*, 2012], the tide/wave nonlinear interactions [e.g., *Sridharan et al.*, 2009; *Fuller-Rowell et al.*, 2011; *Maute et al.*, 2014], and may modify the tidal forcing [e.g., *Goncharenko et al.*, 2012; *Smith*, 2012].

Observed disturbances in the thermosphere [e.g., *Forbes and Zhang*, 2012; *Liu et al.*, 2013, 2014] and ionosphere [e.g., *Chau et al.*, 2009; *Stening*, 2011; *Jonah et al.*, 2014; *Pancheva et al.*, 2012; *Yamazaki*, 2014] could be attributed to SSW events. Numerical models were employed to investigate the vertical coupling between the lower and upper atmosphere [e.g., *Fuller-Rowell et al.*, 2011; *Fang et al.*, 2012; *Pedatella et al.*, 2012; *Jin et al.*, 2012; *Maute et al.*, 2014, 2015].

This study will focus on the equatorial vertical drift. The equatorial vertical drift changes associated with SSW periods can be described as an increase (decrease) in the prenoon (afternoon) vertical E × B drift [e.g., *Chau et al.*, 2009; *Fejer et al.*, 2010; *Anderson and Araujo-Pradere*, 2010; *Rodrigues et al.*, 2011]. Associated with these low-latitude drift changes are the enhancement (depletion) in the total electron content in the equatorial ionization anomaly region [e.g., *Chau et al.*, 2009; *Goncharenko et al.*, 2010a, 2013].

The characteristic SSW equatorial vertical drift changes were linked to changes in the semidiurnal solar and lunar tide in the *E* region [e.g., *Chau et al.*, 2012, and references therein]. Solar semidiurnal tidal changes were observed with enhancements and a phase shift over several days during the SSW periods based on Arecibo wind observations [e.g., *Gong et al.*, 2013], satellite observations [*Wu et al.*, 2011], meteor radar at Tirunelveli in India [e.g., *Sathishkumar and Sridharan*, 2013], and the specular meteor radars at Juliusruh and Andenes [*Chau et al.*, 2015].

The importance of the semidiurnal lunar tide during SSW periods was pointed out by *Stening et al.* [1997] through simulations. During SSW periods enhanced semidiurnal lunar tidal signals were measured in the equatorial vertical drift [e.g., *Fejer et al.*, 2010, 2011], equatorial electrojet [e.g., *Yamazaki et al.*, 2012; *Park et al.*, 2012], and mesospheric winds [e.g., *Paulino et al.*, 2012; *Sathishkumar and Sridharan*, 2013; *Chau et al.*, 2015]. A study by *Forbes and Zhang* [2012] illustrated that the lunar M_2 and N_2 tides can be enhanced by resonance while propagating through the disturbed zonal mean atmosphere as present during SSWs.

A behavior of the vertical drift which was reported on, but to our knowledge the causes were not examined, is the several-day suppression of the daytime equatorial vertical drift preceding and following the several-day vertical drift enhancement. *Goncharenko et al.* [2013] and *Jonah et al.* [2014] pointed out the behavior for the 2013 SSW period. *Fejer et al.* [2010, 2011] observed the suppressed daytime vertical drift periods for warming periods in January 2003 and 2009 in the American, Indian, and Pacific sector. The anomalous low and high drift periods do not necessarily align with the lunar new/full moon.

In this study we focus on the 2013 SSW period for which anomalous low vertical drifts were observed at Jicamarca before and after the daytime drift enhancement. The NCAR thermosphere-ionosphere-mesosphere-electrodynamics general circulation model (TIME-GCM) is employed to examine possible causes of the modulation of the daytime equatorial vertical drift. In section 2 the meteorological and solar wind conditions during January 2013 are described. Section 3 introduces the TIME-GCM simulations before the results are discussed in section 4 and summarized in section 5.

2. The 2013 SSW Period

The prevailing meteorological and geomagnetic conditions during the 2013 SSW period are described in *Maute et al.* [2015] and briefly summarized as follows. During December 2012 the winter polar vortex was shifted off the geographic pole leading to an increased planetary wave 1 (PW1) which then split around 5 January resulting in a strong planetary wave 2 (PW2) peaking around 8 January. At the same time the average polar temperature between 60°–90°geographic latitude at 10 hPa increased between 1 and 10 January up to 25 K above the climatological value. The SSW peaked at 9 January and the recovery of the atmosphere to the seasonal behavior took till end of February. Associated with the SSW is a zonal mean wind weakening in the polar region. The stratospheric winter polar vortex was already less eastward in December 2012 and then turned westward at 10 hPa and 60°geographic latitude around 6 January during the peak of the PW2 activity.

The solar radio flux $F_{10.7}$ was approximately 100 solar flux unit (sfu) (1 sfu $=10^{-22}\mathrm{Wm}^{-2}\mathrm{Hz}^{-1}$) in January 2013 but between 1 and 20 January $F_{10.7}$ increased by up to 70 sfu. January 2013 was geomagnetic quiescent but *Kp* reached values of 4 on 17 and 26 January indicating moderate geomagnetic activity.

The lunar phase is depicted in Figure 1 with new moon occurring on 11 January 2013 and 10 February 2013 and full moon on 28 December 2012 and 27 January 2013.

3. Model Description

The present modeling study builds upon the 2013 SSW simulation described in *Maute et al.* [2015], and the main features are just briefly summarized in the following.

The TIME-GCM is a self-consistent model of the middle and upper atmosphere which includes dynamics, energetics, and chemistry [*Roble and Ridle*, 1994; *Roble*, 1995, 1996] with a self-consistent steady state ionospheric electrodynamo [*Richmond*, 1995]. The TIME-GCM has a horizontal resolution of 2.5°by 2.5°and vertical one of one fourth scale height. At the upper boundary at approximately 450–600 km the O^+ flux and electron heat flux are specified. At the lower boundary (approximately 30 km) the zonal and diurnal mean atmosphere and the tidal and wave perturbations are prescribed based on a Whole Atmosphere Community Climate Model -Extended (WACCMX)-116L/GEOS-5 simulation [*Maute et al.*, 2015]. The TIME-GCM zonal mean neutral

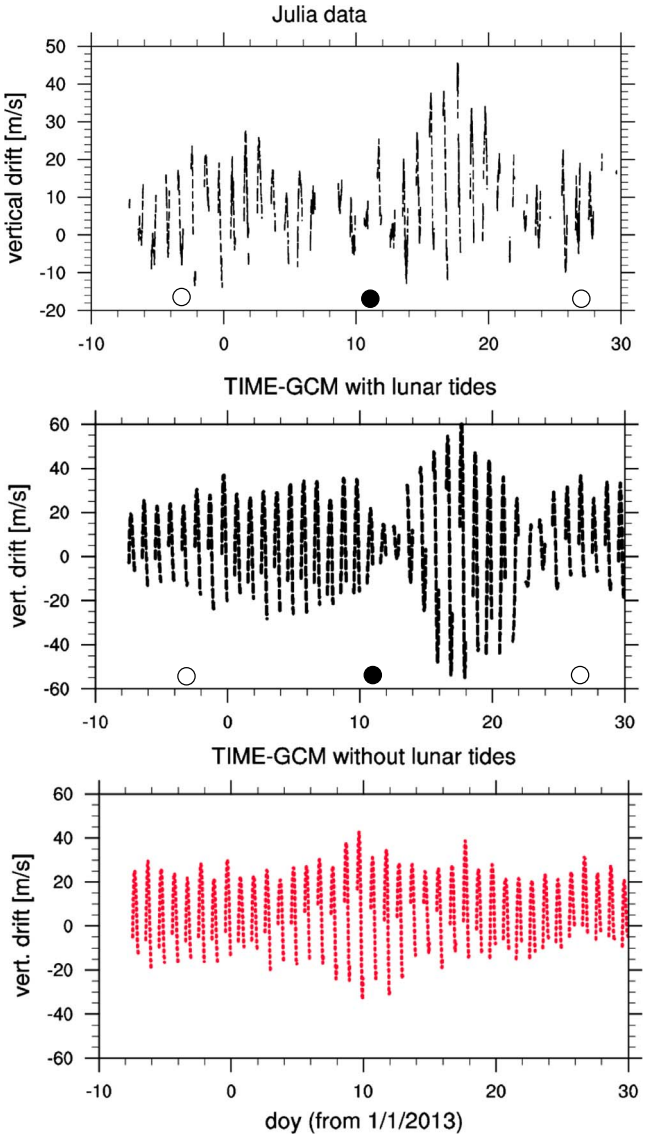

Figure 1. Vertical drift at Jicamarca location between 7 and 18 solar local time over day of the year with 1 January 2013 as day 1: (top) JULIA observations; TIME-GCM E × B drift simulation at approximately 120 km (Z = -4) (middle) with and (bottom) without lunar tidal M_2 and N_2 forcing at the lower boundary. Full moon and new moon are depicted by the white and black circles, respectively, at the bottom of the panels.

horizontal winds and temperatures were nudged by WACCMX-116L/GEOS-5 results with decreasing weighting up to approximately 110 km (logarithmic pressure level Z= $ln(p_o/p) = -5$ with $p_o = 0.005$ mb). Realistic geospace variability of solar radiation and geomagnetic activity was included in the simulation as described in *Maute et al.* [2015].

At the lower boundary of TIME-GCM the lunar tidal perturbations are specified in addition to the solar tidal perturbations and planetary wave forcing which is given by hourly WACCMX-L116/GEOS-5 results. The lunar perturbations at the lower boundary of TIME-GCM are based on the global scale wave model (GSWM-09) [*Zhang et al.*, 2010] simulations forced with the lunar tidal potential while prescribing a realistic zonal mean atmosphere in the modeling domain as described below.

The GSWM solves the linearized tidal equations for a given zonally averaged atmospheric state. GSWM calculates the latitudinal and height variation of user-specified waves for various excitations [e.g., *Hagan et al.*, 1995, 1999; *Hagan and Forbes*, 2002, 2003]. The model includes the important effects in calculating the tidal

response: surface friction, mean winds, and meridional gradients in scalar atmospheric parameters, radiative cooling, eddy and molecular diffusion, Rayleigh friction, and ion drag.

Lunar tidal forcing in GSWM was introduced as described in *Forbes* [1982a, 1982b] and *Forbes et al.* [2013], while the solar thermal forcing was omitted. The atmospheric lunar response depends on the propagation conditions [e.g., *Stening et al.*, 1997; *Forbes and Zhang*, 2012] and a realistic representation of the zonal mean winds and temperatures. The GSWM-09 obtains these zonal means from the Modern Era retrospective-analysis for Research and Applications up to approximately 70 km [*Forbes and Zhang*, 2012]. Above 70 km the zonal means smoothly transit to the monthly climatology based on available observations.

For the present study the TIME-GCM lower boundary is forced by the M_2 and N_2 lunar tidal perturbations based on the GSWM analysis for the 2013 SSW period. The gravitational potential difference between Earth and Moon generates a spectrum of lunar tidal components. The semidiurnal lunar tide M_2 (period is 12.41 h) would be the sole lunar period if the Moon's orbit would be a perfect circle and the Moon and Earth equatorial planes were aligned. The N_2 lunar tidal component arises due to the small eccentricity and angle between the equatorial plane of Earth and Moon. The semidiurnal lunar tide N_2 has a period of 12.66 h. For more details about lunar tidal forcing we refer the reader to *Forbes et al.* [2013].

The present study focuses on the effect of the lunar tidal components on low-latitude ionospheric equatorial vertical drifts. The lunar tidal influence in the simulation is delineated by conducting two simulations: one with lunar tidal forcing at the lower boundary and a control simulation without lunar tidal forcing. The latter was described in *Maute et al.* [2015], but otherwise, the two simulation setups are identical. We term the first "lunar simulation" and the latter "control simulation".

4. Results

The vertical drift from the Jicamarca Unattended Long-term Investigations of the Ionosphere and Atmosphere (JULIA) radar at Jicarmarca, Peru (−11.95°geographic latitude, −76.87°geographic longitude, 1°dip angle), between 7 and 18 local time (LT) is depicted in Figure 1 (top). The daytime vertical drift is enhanced between 15 and 19 January with values up to 43 m/s and reduced between 6–13 January and 22–25 January with maximum daytime values between 0 and 12 m/s [*Goncharenko et al.*, 2013]. The cycle of reduced and enhanced vertical drift periods is not aligned with the lunar full and new moon indicted by the black and white circles at the bottom of the panel, respectively. *Fejer et al.* [2010, 2011] noted a 4–6 days shift between vertical drift enhancement and lunar full/new moon.

The "control" TIME-GCM simulation [*Maute et al.*, 2015] (see Figure 1, bottom) cannot reproduce the modulation of the daytime vertical drift as observed by JULIA. However, this simulation was able to reproduce the observed local time shift of the daytime maximum drift from prenoon to the afternoon between 15 and 20 January as illustrated in Figure 5 of *Maute et al.* [2015].

Including lunar tidal forcing at the lower boundary of TIME-GCM leads to a similar modulation of the daytime vertical drift as observed (see Figure 1 middle) with reduced drift periods between 11–14 and 22–24 January around 10 days apart. The timing of the simulated enhanced drift period starting around 16 January agrees with the findings by *Fejer et al.* [2011] that the vertical drift is enhanced 4–6 days after the new or full moon.

The diurnal drift variation is provided in Figure 2 for specific days. Figures 2a and 2b display examples for the reduced drift phase for 12 and 23 January, respectively. Figures 2c, 2d, and 2e are examples for the enhanced drift period with 16, 17, and 18 January, respectively. The control simulation (red lines) captures better the magnitude of the observed drift than the lunar simulation (black line) during the enhanced drift period. But the control simulation cannot reproduce the reduced drift before and after the enhanced drift period. The local time of the daytime maximum drift is more accurately captured by the lunar simulation especially for the reduced vertical drift period (Figures 2a and 2b). Note that on 17 January the observed vertical drift is geomagnetically disturbed, with a *Kp* index of 4 between 15 and 18 universal time (10–13 LT).

The zonal wind amplitude at approximately 120 km is depicted in Figures 3a–3c for the solar semidiurnal migrating tide SW_2 (Figures 3a, 3, and 3g) and the lunar tide M_2 (Figures 3b, 3e, and 3h) based on the "lunar" simulation with M_2 and N_2 lunar tidal forcing at lower boundary. In Figures 3c, 3f, and 3i the lunar tide M_2 based on a comparison simulation with M_2 lunar tidal forcing (omitting the N_2 forcing) at lower boundary is illustrated. The meridional wind amplitude behaves similarly to the zonal wind amplitude, and therefore, it is

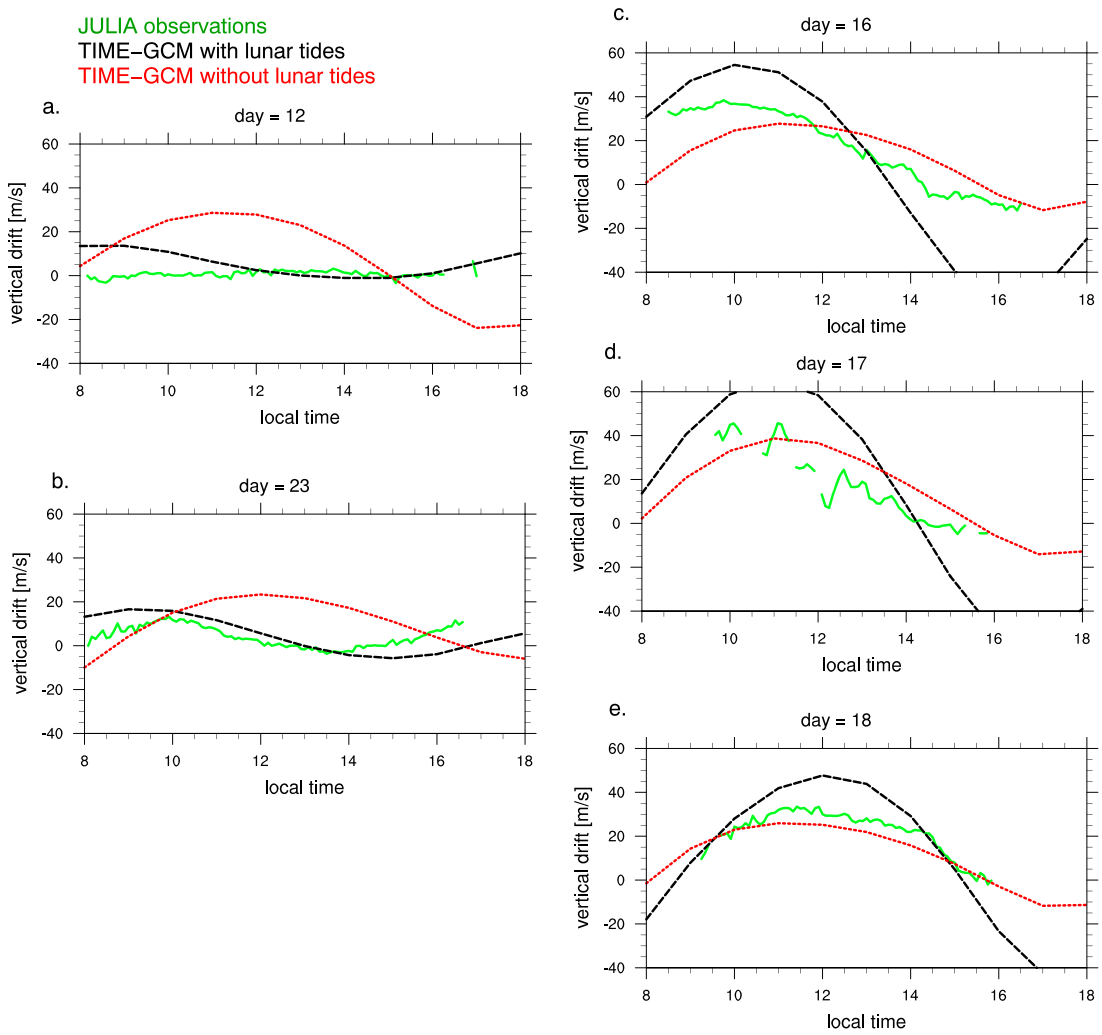

Figure 2. Vertical drift at Jicamarca between 8 and 18 solar local time for day 12, 23, 16, 17, and 18 based on JULIA observation (green line), TIME-GCM with and without lunar M_2 and N_2 forcing (black and red lines, respectively).

not illustrated or discussed separately in this study. However, it is noted that both the zonal and meridional winds contribute to the equatorial vertical drift [e.g., *Heelis*, 2004; *Liu and Richmond*, 2013], and the zonal wind component is illustrated as an example.

Since the periods of SW_2, M_2, and N_2 are similar, a 14.5 day window was used on the detrended (removing a constant and linear term) zonal wind to delineate the solar and lunar semidiurnal components SW_2 and M_2. However, even with a 14.5 day window, the lunar M_2 and N_2 cannot be fully separated since the periods differ by only 0.25 h. The influence of the N_2 lunar component on the derived M_2 tidal amplitude is estimated by a comparison simulation which is identical to the lunar simulation except that it omits the lunar N_2 tidal forcing at the lower boundary. Results of the comparison simulation are shown in Figures 3c, 3f, and 3i. The M_2 amplitude variation in Figures 3b and 3c are very similar indicating that the N_2 lunar tide has only a minor influence on the zonal wind in the *E* region.

During 10–25 January the lunar M_2 and solar SW_2 tidal amplitudes are comparable in magnitude. As shown by *Forbes and Zhang* [2012] for the 2009 SSW, the lunar M_2 tidal component during the 2013 SSW is amplified at the background atmosphere Pekeris resonance frequency.

Although the semidiurnal solar and lunar tidal forcing at the lower boundary tends to be stronger in the Northern Hemisphere (Figures 3g and 3h), in the *E* region the solar and lunar semidiurnal amplitudes are stronger in the Southern Hemisphere. This may be caused by hemispheric differences in the middle atmosphere background through which the tides propagate, exciting asymmetric tidal modes which then

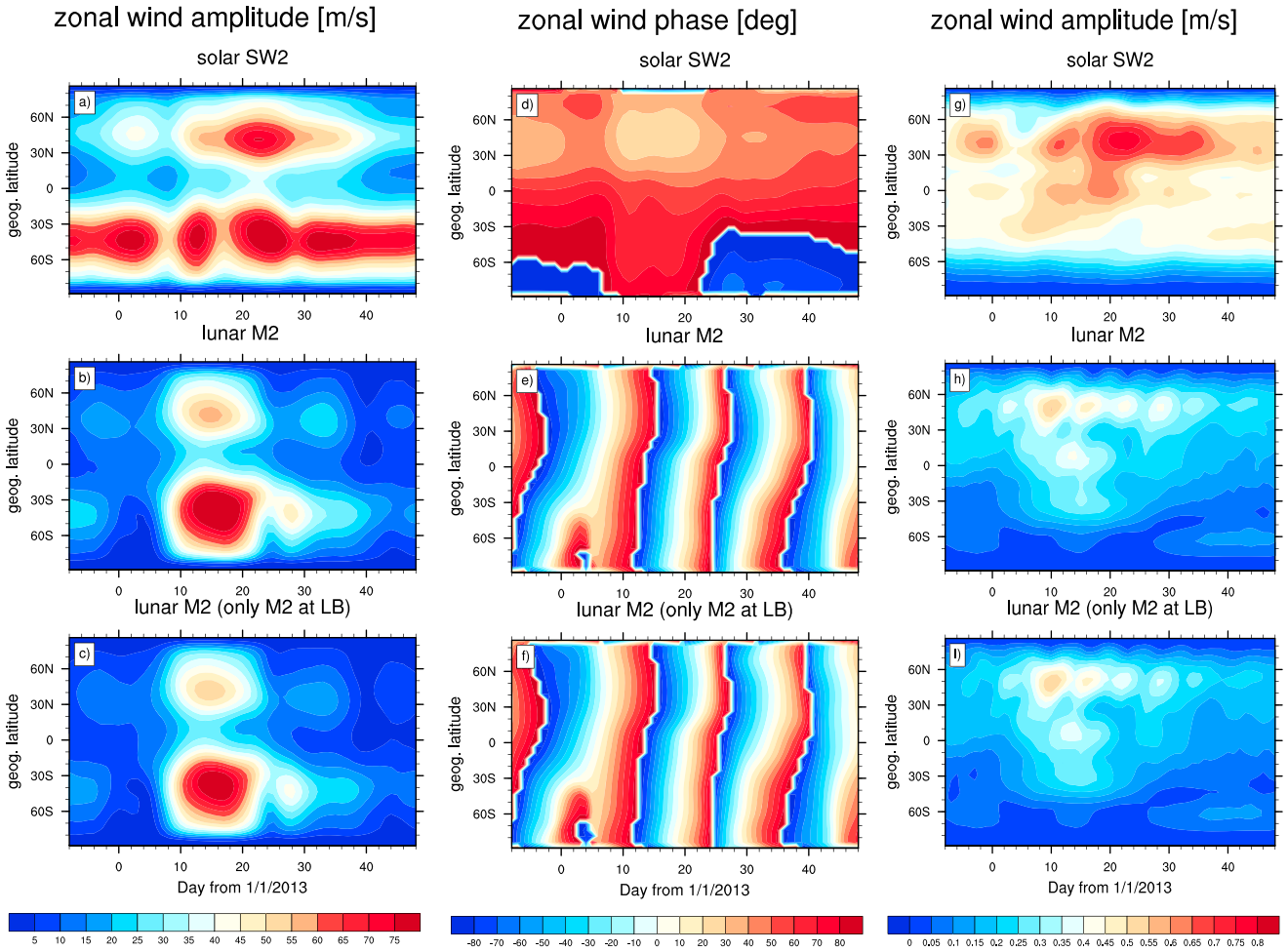

Figure 3. Zonal wind amplitudes (m/s) at (a–c) approximately 120 km and at (g–i) lower boundary (approximately 30 km). (d–f) Zonal wind phase defined as the longitude (degrees) of maximum at 0 UT at approximately 120 km for solar semidiurnal migrating tide SW_2 (Figures 3a, 3d, and 3g), lunar semidiurnal M_2 tide for simulation which includes lunar tidal components M_2 and N_2 at lower boundary (Figures 3b, 3e, and 3h), and simulation which includes only lunar tidal component M_2 at the lower boundary (Figures 3c, 3f, and 3i). Amplitudes and phases are determined by a least squares fit with a 14.5 day running window applied to the detrended temporal variation.

propagate into the thermosphere [*Forbes et al.*, 2013]. The control simulation shows larger SW_2 amplitudes in the Southern Hemisphere as well (not illustrated) indicating that the hemispheric difference is not caused by the inclusion of the lunar tides at the lower boundary.

The zonal wind amplitudes (Figures 3a and 3b) exhibit a strong periodicity of around 7 to 15 days for SW_2 and around 10 to 15 days for M_2 most prominent in the Southern Hemisphere between 1 and 25 January. Spectral analysis of the planetary waves at the lower boundary of the TIME-GCM indicates a 7 to 15 days periodicity in the planetary waves with zonal wave number 1 and 2 most pronounced in the Northern Hemisphere between 1 and 20 January, which could lead to the modulation of the semidiurnal tides as seen in the *E* region.

The low-amplitude periods for SW_2 and M_2 in the *E* region (Figures 3a and 3b) do not align with the reduced drift periods (11–14 and 22–24 January in Figure 1). SW_2 amplitudes maximize between 10–15 January and 20–25 January, and the M_2 amplitudes are maximum between 10 and 20 January.

The phases corresponding to the amplitudes (Figures 3a and 3b) are depicted in Figures 3d and 3e. During the 11–14 January minimum drift period SW_2 and M_2 tides have similar large amplitudes and are almost in phase (10°–30° difference), while during 22–24 January SW_2 amplitude is larger than M_2 with a phase difference of 10°–30° at the latitudes of strong amplitude. During the maximum daytime drift period 16–20 January SW_2 and M_2 tides tend to be out of phase.

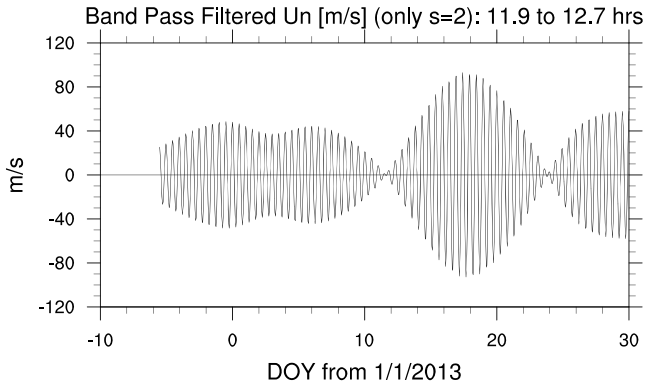

Figure 4. Band-pass filter of zonal wind with zonal wave number 2 at −45° geographic latitude, approximately 120 km and 90° geographic longitude for periods between 11.9 and 12.7 h.

Based on the presented phase analysis, the modulation of the daytime vertical drift cannot be fully explained by the temporal variation of SW_2 and M_2 tidal amplitudes and phases. However, caution in the interpretation of the tidal analysis is warranted since a 14.5 day processing window was applied to delineate the tidal components, and therefore, temporal smoothing is present (see discussion and numerical experiments in *Maute et al.* [2015]).

To capture the combined SW_2 and M_2 tidal effect, we applied a band-pass filter to the zonal wind at $Z = -4$ (approximately 120 km) for periods from 11.9 to 12.7 h at −45° geographic latitude (see Figure 4). Since other semidiurnal tidal components could be present, we used only the wind based on zonal wave number 2. This eliminates the westward propagating semidiurnal tide with zonal wave number 1 (SW1) which is strong in the high-latitude region (up to 22 m/s) but weaker at midlatitude (−45° geographic latitude) with a maximum of 15 m/s between 1 and 15 January in the lunar simulation. Therefore, the effect of SW1 on the band-pass filtered wind would be minor.

In Figure 4 there are pronounced minima of the band-pass filtered zonal wind centered around 12 and 24 January and a secondary one at 3 January. These results suggest that the temporal variation of the semidiurnal solar and lunar tides cause the modulation of the vertical drift at Jicamarca. Two waves with frequencies f_1 and f_2 and amplitudes a_1 and a_2 can cause a "beating" frequency of $f_{beat} = f_1 - f_2$ and amplitude variations between $|a_1 + a_2|$ and $|a_1 - a_2|$.

Tidal amplitudes of SW_2 and M_2 are comparable in magnitude suggesting that the beating amplitude may be large enough to be observable. If the tidal phases did not vary in time, the beating frequency of SW_2 and M_2 would be $f_{beat} = 1/(15.13 \text{ day})$. While the phase of SW_2 varies slowly in time, the M_2 phases shift by 180° in approximately 12 days during 10–25 January (Figure 3). These phase shifts can modify the theoretical beating frequency which would also explain that the amplitude variation (between approximately 0 to 93 m/s) is different from the theoretical value of $|a_1 + a_2|$ of roughly 135 m/s with SW_2 and M_2 amplitudes around 55 m/s and 80 m/s, respectively, at 18 January and $|a_1 - a_2|$ of roughly 5 m/s with SW_2 and M_2 amplitude of around 70 m/s and 75 m/s, respectively, at 12 January for southern midlatitudes.

The secondary minimum at 3 January in the band-pass filtered zonal wind can be explained by the much smaller amplitudes of M_2 compared to SW_2 during that time period indicating that although beating should be present all the time, the effect is only observable when the amplitudes are significant and comparable in size.

As expected the simulation indicates that the effects of the SW_2 and M_2 beating should be observable at all longitudes as illustrated in Figure 5 for the African and Asian sectors. The reduced daytime equatorial vertical drift periods between 11–14 and 22–24 January and the enhanced drift period between 16 and 20 January align with the ones for Jicamarca in the American sector. The vertical drift modulation due to the beating is large enough to expect ionospheric changes. However, delineating the ionospheric effects due to the beating of the waves from ionospheric changes due to modified dynamics and composition caused by the inclusion of the lunar tides in the simulation is challenging and not within the scope of the present study.

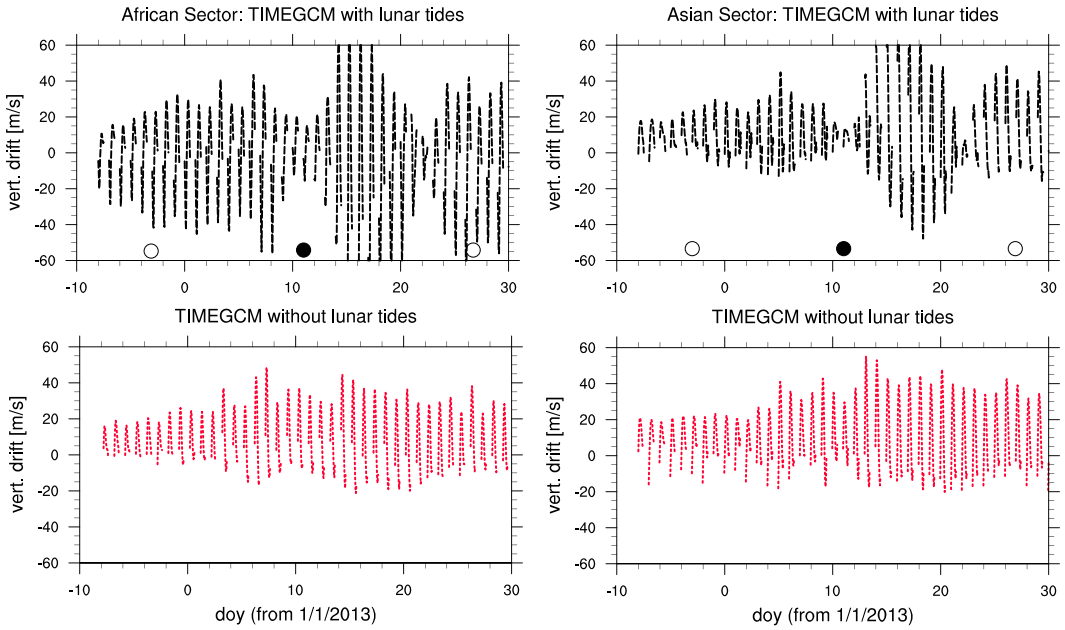

Figure 5. Equatorial vertical E × B drift between 7 and 18 solar local time over day of the year with 1 January 2013 as day 1 based on TIME-GCM simulations at approximately 120 km (Z= -4) (top rows) with and (bottom rows) without lunar tidal M_2 and N_2 forcing at the lower boundary for the (first column) African sector (8.75°geographic latitude, 40°geographic longitude) and the (second column) Asian sector (8.75°geographic latitude, 120°geographic longitude). Full moon and new moon are depicted by the white and black circles, respectively, in Figure 5.

5. Conclusions

This study examines the modulation of the daytime equatorial vertical drift during the 2013 SSW which was observed by JULIA. *Goncharenko et al.* [2013] noted unusually reduced daytime drifts before and after the main enhanced vertical drift period at Jicarmarca. Using the TIME-GCM, the present study examined the causes of this modulation. The main findings are summarized in the following.

The TIME-GCM simulation indicates that the daytime vertical drift modulation is caused by the interplay of the semidiurnal lunar (M_2) and solar (SW_2) tides. The simulation without lunar tidal forcing cannot reproduce this modulation. Adding lunar tidal forcing at the lower boundary leads to improved day-to-day variation of the daytime maximum vertical drift and more accurate diurnal drift variation with respect to the observation. Especially during the reduced drift period (11–14 and 22–24 January), the simulated daytime drift compares favorably with the observations with respect to magnitude and local time of the daytime drift.

Associated with the SSW is the shift of the daytime maximum vertical drift from prenoon to the afternoon [e.g., *Chau et al.*, 2009; *Goncharenko et al.*, 2010b, 2010a; *Fejer et al.*, 2010; *Anderson and Araujo-Pradere*, 2010; *Jonah et al.*, 2014] over several days which happens during the enhanced drift phase and can be reproduced by numerical models using only solar tidal forcing if SW_2 has the right phase shift [e.g., *Fuller-Rowell et al.*, 2011; *Jin et al.*, 2012; *Maute et al.*, 2015]. However, the modulation of the vertical drift examined in the present study can only be reproduced by including solar and lunar tidal forcing. In the lunar simulation the daytime vertical drift is overestimated compared to the magnitude of the observed drift, but the diurnal variation is captured more accurately compared to the control simulation.

Diagnostics of the simulation suggest that the modulation of the vertical drift is caused by the beating of SW_2 and M_2 tides. Analyzing the temporal and spatial variation of the amplitude and phase of SW_2 and M_2 did not indicate that a phase shift is responsible for the modulation of the vertical drift, although the interpretation of the amplitude and phase is difficult due to the 14.5 day processing window. Filtering the zonal wind for the periods of quasi 12 h revealed a very similar modulation, as the equatorial vertical drift exhibits with pronounced low and high zonal wind periods.

The theoretical beating frequency of SW_2 and M_2 is $f_{beat} = 1/(15.13\ \text{day})$ if the tidal phases are not varying over time. Especially, M_2 phase is changing considerably in time, and therefore, the beating frequency can

be shifted to longer and shorter periods. Indicative of the influence of phase change is that the difference in amplitude maxima between reduced and enhanced zonal wind periods is smaller than the theoretical value of the sum and differences between the solar and lunar tidal amplitudes of M_2 and SW_2.

The simulated daytime vertical drift during the enhanced drift period is overestimated compared to the observations. The results suggest that both lunar (M_2) and solar (SW_2) semidiurnal tidal components are overestimated since comparable amplitudes are needed to get a modulation of the vertical drift by the beating of these components. A reduced but less pronounced zonal wind magnitude was illustrated around 3 January in the band-pass wind field which is supported by the reduced M_2 tidal amplitudes compared to the SW_2 amplitudes, leading to a weaker modulation of the zonal wind due to beating.

Several observations not directly pertaining to the vertical drifts modulation at Jicamarca can be made and are summarized below.

The lunar tidal amplitude M_2 is amplified during the SSW period in the TIME-GCM simulation which agrees with results by *Forbes and Zhang* [2012]. At the lower boundary the lunar tidal forcing tends to be stronger in the Northern Hemisphere, but in the *E* region tidal, amplitudes of SW_2 and M_2 are more pronounced in the Southern Hemisphere. Hemispheric differences in the zonal mean middle atmosphere could influence the propagation condition and favor the propagation and/or amplification in one hemisphere. Further examination of the hemispheric differences is not within the scope of the present study.

In the *E* region SW_2 and M_2 amplitudes exhibit a quasi 7–15 day periodicity which might be caused by a quasi 7–15 day planetary wave modulation with zonal wave numbers 1 and 2 at the lower boundary of the model (approximately 30 km). A separate study will be conducted focusing on the neutral dynamics during the SSW period.

With respect to the modulation of the vertical drift during SSW period several open questions remain which should be addressed by modeling and observational studies. The simulation indicates that all longitudes exhibit the modulation of the vertical drift. Daytime vertical drift at the magnetic equator based on magnetometer data can be used to examine if the modulation is manifested at all longitudes. It is feasible that the strong modulation of the vertical drift has effects on the ionosphere and may be observable in N_mF_2, h_mF_2, and total electron content.

The modulation of the vertical drift is only strong if the semidiurnal lunar and solar tides have similar amplitudes. During non-SSW periods a modulation may occur, but it is weaker, and therefore, it is more difficult to delineate this effect from other variations. Future work includes studying different SSW periods with focus on the modulation of the vertical drift to address if there is some commonality between different SSW periods or if the 2013 SSW drift modulation was unique.

Acknowledgments
TIME-GCM results are archived on the National Center for Atmospheric Research High Performance Storage System and are available on request. We would like to acknowledge high-performance computing support from Yellowstone (ark:/85065/d7wd3xhc) provided by NCAR's Computational and Information Systems Laboratory, sponsored by the National Science Foundation. A.M. would like to thank Art Richmond for the helpful comments on an earlier draft. A.M. was supported in part by NASA grant NNX13AF77G. The National Center for Atmospheric Research is sponsored by the National Science Foundation. J.M. Forbes and X. Zhang were supported by NASA award NNX12AJ58G under the Heliophysics Guest Investigator Program. The work at Utah State University was supported by NSF grant AGS-1068104. V.A. Yudin was supported by NASA award NNX14AI17G and NSF/CEDAR grant AGS-1343031. The Jicamarca Radio Observatory is a facility of the Instituto Geofsico del Peru operated with support from NSF award AGS-0905448 through Cornell. JRO data used for this publication are available through the Madrigal database.

References

Anderson, D., and E. A. Araujo-Pradere (2010), Sudden stratospheric warming event signatures in daytime E × B drift velocities in the Peruvian and Philippine longitude sectors for January 2003 and 2004, *J. Geophys. Res.*, *115*, A00G05, doi:10.1029/2010JA015337.

Chau, J., B. G. Fejer, and L. P. Goncharenko (2009), Quiet variability of equatorial E × B drifts during a sudden stratospheric warming event, *Geophys. Res. Lett.*, *36*, L05101, doi:10.1029/2008GL036785.

Chau, J., L. P. Goncharenko, B. G. Fejer, and H.-L. Liu (2012), Equatorial and low latitude ionospheric effects during sudden stratospheric warming events, *Space Sci. Rev.*, *168*, 385–417, doi:10.1007/s11214-011-9797-5.

Chau, J. L., P. Hoffmann, N. M. Pedatella, V. Matthias, and G. Stober (2015), Upper mesospheric lunar tides over middle and high latitudes during sudden stratospheric warming events, *J. Geophys. Res. Space Physics*, *120*, 3084–3096, doi:10.1002/2015JA020998.

England, S. L. (2012), A review of the effects of non-migrating atmospheric tides on the Earth's low-latitude ionosphere, *Space Sci. Rev.*, *168*(1), 211–236.

Fang, T.-W., T. Fuller-Rowell, R. Akmaev, F. Wu, H. Wang, and D. Anderson (2012), Longitudinal variation of ionospheric vertical drifts during the 2009 sudden stratospheric warming, *J. Geophys. Res.*, *117*, A03324, doi:10.1029/2011JA017348.

Fejer, B., M. E. Olson, J. L. Chau, C. Stolle, H. Lühr, L. P. Goncharenko, K. Yumoto, and T. Nagatsuma (2010), Lunar-dependent equatorial ionospheric electrodynamic effects during sudden stratospheric warmings, *J. Geophys. Res.*, *115*, A00G03, doi:10.1029/2010JA015273.

Fejer, B. G., B. D. Tracy, M. E. Olson, and J. L. Chau (2011), Enhanced lunar semidiurnal equatorial vertical plasma drifts during sudden stratospheric warmings, *Geophys. Res. Lett.*, *38*, L21104, doi:10.1029/2011GL049788.

Forbes, J. M. (1982a), Atmospheric tides: 1. Model description and results for the solar diurnal component, *J. Geophys. Res.*, *87*(A7), 5222–5240, doi:10.1029/JA087iA07p05222.

Forbes, J. M. (1982b), Atmospheric tide: 2. The solar and lunar semidiurnal components, *J. Geophys. Res.*, *87*(A7), 5241–5252, doi:10.1029/JA087iA07p05241.

Forbes, J. M., and X. Zhang (2012), Lunar tide amplification during the January 2009 stratosphere warming event: Observations and theory, *J. Geophys. Res.*, *117*, A12312, doi:10.1029/2012JA017963.

Forbes, J. M., X. Zhang, S. Bruinsma, and J. Oberheide (2013), Lunar semidiurnal tide in the thermosphere under solar minimum conditions, *J. Geophys. Res. Space Physics*, *118*, 1788–1801, doi:10.1029/2012JA017962.

Fuller-Rowell, T., R. Akmaev, F. Wu, T.-W. Fang, M. Iredell, and A. Richmond (2011), Forecasting the dynamic and electrodynamic response to the January 2009 sudden stratospheric warming, *Geophys. Res. Lett.*, *38*, L13102, doi:10.1029/2011GL047732.

Goncharenko, L., and S.-R. Zhang (2008), Ionospheric signatures of sudden stratospheric warming: Ion temperature at middle latitude, *Geophys. Res. Lett.*, *35*, L21103, doi:10.1029/2008GL035684.

Goncharenko, L., A. J. Coster, J. L. Chau, and C. E. Valladares (2010a), Impact of sudden stratospheric warmings on equatorial ionization anomaly, *J. Geophys. Res.*, *115*, A00G07, doi:10.1029/2010JA015400.

Goncharenko, L., J. L. Chau, H.-L. Liu, and A. J. Coster (2010b), Unexpected connections between the stratosphere and ionosphere, *Geophys. Res. Lett.*, *37*, L10101, doi:10.1029/2010GL043125.

Goncharenko, L., A. J. C. R. A. Plumb, and D. I. V. Domeisen (2012), The potential role of stratospheric ozone in the stratosphere-ionosphere coupling during stratospheric warmings, *Geophys. Res. Lett.*, *39*, L08101, doi:10.1029/2012GL051261.

Goncharenko, L., J. L. Chau, P. Condor, A. Coster, and L. Benkevitch (2013), Ionospheric effects of sudden stratospheric warming during moderate-to-high solar activity: Case study of January 2013, *Geophys. Res. Lett.*, *40*, 4982–4986, doi:10.1002/grl.50980.

Gong, Y., Q. Zhou, and S. Zhang (2013), Atmospheric tides in the low-latitude E and F regions and their responses to a sudden stratospheric warming event in January 2010, *J. Geophys. Res. Space Physics*, *118*, 7913–7927, doi:10.1002/2013JA019248.

Hagan, M. E., and J. M. Forbes (2002), Migrating and nonmigrating diurnal tides in the middle and upper atmosphere excited by tropospheric latent heat release, *J. Geophys. Res.*, *107*(D24), 4754, doi:10.1029/2001JD001236.

Hagan, M. E., and J. Forbes (2003), Migrating and nonmigrating semidiurnal tides in the upper atmosphere excited by tropospheric latent heat release, *J. Geophys. Res*, *108*(A2), 1062, doi:10.1029/2002JA009466.

Hagan, M. E., J. M. Forbes, and F. Vial (1995), On modeling migrating solar tides, *Geophys. Res. Lett.*, *22*(8), 893–896, doi:10.1029/95GL00783.

Hagan, M. E., M. D. Burrage, J. M. Forbes, J. Hackney, W. J. Randel, and X. Zhang (1999), GSWM-98: Results for migrating solar tides, *J. Geophys. Res.*, *104*(A4), 6813–6827, doi:10.1029/1998JA900125.

Heelis, R. A. (2004), Electrodynamics in the low and middle latitude ionosphere: A tutorial, *J. Atmos. Sol. Terr. Phys.*, *66*, 825–838, doi:10.1016/j.jastp.2004.01.034.

Jin, H., Y. Miyoshi, D. Pancheva, P. Mukhtarov, H. Fujiwara, and H. Shinagawa (2012), Response of migrating tides to the stratospheric sudden warming in 2009 and their effects on the ionosphere studied by a whole atmosphere-ionosphere model GAIA with COSMIC and TIMED/SABER observations, *J. Geophys. Res.*, *117*, A10323, doi:10.1029/2012JA017650.

Jonah, O. F., E. R. de Paula, E. A. Kherani, S. L. G. Dutra, and R. R. Paes (2014), Atmospheric and ionospheric response to sudden stratospheric warming of January 2013, *J. Geophys. Res. Space Physics*, *119*, 4973–4980, doi:10.1002/2013JA019491.

Lin, C. H., J. T. Lin, L. C. Chang, J. Y. Liu, C. H. Chen, W. H. Chen, H. H. Huang, and C. H. Liu (2012), Observations of global ionospheric responses to the 2009 stratospheric sudden warming event by FORMOSAT-3/COSMIC, *J. Geophys. Res.*, *117*, A06323, doi:10.1029/2011JA017230.

Liu, H., H. Jin, Y. Miyoshi, H. Fujiwara, and H. Shinagawa (2013), Upper atmosphere response to stratosphere sudden warming: Local time and height dependence simulated by GAIA model, *Geophys. Res. Lett.*, *40*, 635–640, doi:10.1002/grl.50146.

Liu, H., Y. Miyoshi, S. Miyahara, H. Jin, H. Fujiwara, and H. Shinagawa (2014), Thermal and dynamical changes of the zonal mean state of the thermosphere during the 2009 SSW: GAIA simulations, *J. Geophys. Res. Space Physics*, *119*, 6784–6791, doi:10.1002/2014JA020222.

Liu, H.-L., and A. D. Richmond (2013), Attribution of ionospheric vertical plasma drift perturbations to large-scale waves and the dependence on solar activity, *J. Geophys. Res. Space Physics*, *118*, 2452–2465, doi:10.1002/jgra.50265.

Matsuno, T. (1971), A dynamical model of the stratospheric sudden warming, *J. Atmos. Sci.*, *28*(8), 1479–1494.

Maute, A., M. E. Hagan, A. D. Richmond, and R. G. Roble (2014), TIME-GCM study of the ionospheric equatorial vertical drift changes during the 2006 stratospheric sudden warming, *J. Geophys. Res. Space Physics*, *119*, 1287–1305, doi:10.1002/2013JA019490.

Maute, A., M. Hagan, V. Yudin, H.-L. Liu, and E. Yizengaw (2015), Causes of the longitudinal differences in the equatorial vertical ExB drift during the 2013 SSW period as simulated by the TIME-GCM, *J. Geophys. Res. Space Physics*, *120*, 5117–5136, doi:10.1002/2015JA021126.

Pancheva, D., Y. Miyoshi, P. Mukhtarov, H. Jin, H. Shinagawa, and H. Fujiwara (2012), Global response of the ionosphere to atmospheric tides forced from below: Comparison between COSMIC measurements and simulations by atmosphere-ionosphere coupled model GAIA, *J. Geophys. Res.*, *117*, A07319, doi:10.1029/2011JA017452.

Park, J., H. Lühr, M. Kunze, B. G. Fejer, and K. W. Min (2012), Effect of sudden stratospheric warming on lunar tidal modulation of the equatorial electrojet, *J. Geophys. Res.*, *117*, A03306, doi:10.1029/2011JA017351.

Paulino, A., P. P. Batista, B. Clemesha, R. Buriti, and N. Schuch (2012), An enhancement of the lunar tide in the MLT region observed in the Brazilian sector during 2006 SSW, *J. Atmos. Sol. Terr. Phys.*, *90*, 97–103, doi:10.1016/j.jastp.2011.12.015.

Pedatella, N., and J. M. Forbes (2010), Evidence for stratosphere sudden warming-ionosphere coupling due to vertically propagating tides, *Geophys. Res. Lett.*, *37*, L11104, doi:10.1029/2010GL043560.

Pedatella, N., H.-L. Liu, A. D. Richmond, A. Maute, and T.-W. Fang (2012), Simulations of solar and lunar tidal variability in the mesosphere and lower thermosphere during sudden stratosphere warmings and their influence on the low-latitude ionosphere, *J. Geophys. Res.*, *117*, A08326, doi:10.1029/2012JA017858.

Richmond, A. (1995), Ionospheric electrodynamics, in *Handbook of Atmospheric Electrodynamics,* vol. 2, edited by H. Volland, pp. 249–290, CRC Press Inc., Boca Raton, Fla.

Roble, R. (1995), Energetics of the mesosphere and thermosphere, in *The Upper Mesosphere and Lower Thermosphere: A Review of Experiment and Theory*, edited by R. M. Johnson and T. L. Killeen, pp. 1–22, AGU, Washington, D. C.

Roble, R. (1996), The NCAR thermosphere-Ionosphere-mesophere-electrodynamics general circulation model (TIME-GCM), in *Solar-Terrestrial Energy Program: Handbook of ionospheric Models*, edited by R. Schunk, pp. 281–288, Utah State Univ., Utah.

Roble, R., and E. Ridle (1994), A thermosphere-ionosphere-mesopshere-electrodynamics general circulation model TIME-GCM: Equinox solar cycle minimum simulations (30–500km), *Geophys. Res. Lett.*, *21*, 417–420, doi:10.1029/93GL03391.

Rodrigues, F., G. Crowley, S. M. I. Azeem, and R. A. Heelis (2011), C/NOFS observations of the equatorial ionospheric electric field response to the 2009 major sudden stratospheric warming event, *J. Geophys. Res.*, *116*, A09316, doi:10.1029/2011JA016660.

Sathishkumar, S., and S. Sridharan (2013), Lunar and solar tidal variabilities in mesospheric winds and EEJ strength over Tirunelveli (8.7oN, 77.8oE) during the 2009 major stratospheric warming, *J. Geophys. Res. Space Physics*, *118*, 533–541, doi:10.1029/2012JA018236.

Smith, A. (2012), Global dynamics of the MLT, *Surv. Geophys.*, *33*, 1177–1230, doi:10.1007/s10712-012-9196-9.

Sridharan, S., S. Sathishkumar, and S. Gurubaran (2009), Variabilities of mesospheric tides and equatorial electrojet strength during major stratospheric warming events, *Ann. Geophys.*, *27*(11), 4125–4130, doi:10.5194/angeo-27-4125-2009.

Stening, R. (2011), Lunar tide in the equatorial electrojet in relation to stratospheric warmings, *J. Geophys. Res.*, *116*, A12315, doi:10.1029/2011JA017047.

Stening, R. J., J. M. Forbes, M. E. Hagan, and A. D. Richmond (1997), Experiments with a lunar atmospheric tidal model, *J. Geophys. Res.*, *102*(D12), 13,465–13,471, doi:10.1029/97JD00778.

Vineeth, C., T. K. Pant, and R. Sridharan (2009), Equatorial counter electrojets and polar stratospheric sudden warmings—A classical example of high latitude-low latitude coupling?, *Ann. Geophys.*, *27*, 3147–3153.

Wu, Q., D. Ortland, S. Solomon, W. Skinner, and R. Niciejewski (2011), Global distribution, seasonal, and inter-annual variations of mesospheric semidiurnal tide observed by TIMED-TIDI, *J. Atmos. Sol. Terr. Phys.*, *73*(17–18), 2482–2502, doi:10.1016/j.jastp.2011.08.007.

Yamazaki, Y. (2014), Solar and lunar ionospheric electrodynamic effects during stratospheric sudden warmings, *J. Atmos. Sol. Terr. Phys.*, *119*, 138–146, doi:10.1016/j.jastp.2014.08.001.

Yamazaki, Y., A. D. Richmond, and K. Yumoto (2012), Stratospheric warmings and the geomagnetic lunar tide: 1958–2007, *J. Geophys. Res.*, *117*, A04301, doi:10.1029/2012JA017514.

Zhang, X., J. M. Forbes, and M. E. Hagan (2010), Longitudinal variation of tides in the mlt region: 2. Relative effects of solar radiative and latent heating, *J. Geophys. Res.*, *115*, A06317, doi:10.1029/2009JA014898.